PCCP

PAPER

View Article Online
View Journal | View Issue

Cite this: *Phys. Chem. Chem. Phys.*, 2017, **19**, 28885

Revealing vilazodone's binding mechanism underlying its partial agonism to the 5-HT_{1A} receptor in the treatment of major depressive disorder†

Guoxun Zheng,[ab] Weiwei Xue,*[a] Fengyuan Yang,[ab] Yang Zhang,[ab] Yuzong Chen,[c] Xiaojun Yao[d] and Feng Zhu *[ab]

Received 20th August 2017,
Accepted 6th October 2017

DOI: 10.1039/c7cp05688e

rsc.li/pccp

It has been estimated that major depressive disorder (MDD) will become the second largest global burden among all diseases by 2030. Various types of drugs, including selective serotonin reuptake inhibitors (SSRIs), serotonin-norepinephrine reuptake inhibitors (SNRIs), and serotonin receptor partial agonist/reuptake inhibitors (SPARIs), have been approved and become the primary or first-line medications prescribed for MDD. SPARI was expected to demonstrate more enhanced drug efficacy and a rapid onset of action as compared to SSRI and SNRI. As one of the most famous SPARIs, vilazodone was approved by the FDA for the treatment of MDD. Because of the great clinical importance of vilazodone, its binding mechanism underlying its partial agonism to the 5-HT_{1A} receptor (5-HT_{1A}R) could provide valuable information to SPARIs' drug-like properties. However, this mechanism has not been reported to date; consequently, the rational design of new efficacious SPARI-based MDD drugs is severely hampered. To explore the molecular mechanism of vilazodone, an integrated computational strategy was adopted in this study to reveal its binding mechanism and prospective structural feature at the agonist binding site of 5-HT_{1A}R. As a result, 22 residues of this receptor were identified as hotspots, consistently favoring the binding of vilazodone and its analogues, and a common binding mechanism underlying their partial agonism to 5-HT_{1A}R was, therefore, discovered. Moreover, three main interaction features between vilazodone and 5-HT_{1A}R have been revealed and schematically summarized. In summary, this newly identified binding mechanism will provide valuable information for medicinal chemists working in the field of rational design of novel SPARIs for MDD treatment.

Introduction

It has been estimated that major depressive disorder (MDD) will become the second largest global burden among all diseases by 2030,[1–3] which makes the discovery of novel and efficacious antidepressants an urgent need.[4–6] Abnormality in the concentrations of monoamine, particularly 5-HT (5-hydroxytryptamine, serotonin) in MDD patients, led to the hypothesis that a dysfunction of 5-HT signaling might cause depression.[7–9] Based on these theories, a variety of drugs have been approved by the food and drug administration (FDA) and become the primary or first-line medications prescribed for MDD.[10–13] These drugs include the selective serotonin reuptake inhibitors (SSRIs),[10,11] serotonin-norepinephrine reuptake inhibitors (SNRIs),[14] and serotonin receptor partial agonist/reuptake inhibitors (SPARIs).[15]

The major problems of both SSRIs and SNRIs are their greatly delayed onset of action and undesired side effects,[16] which substantially hamper their prescription for MDD treatment.[17] The evidence demonstrates that the pre- and post-synaptic 5-HT_{1A} receptors play opposite roles in depression.[18,19] In particular, the activation of pre-synaptic 5-HT_{1A}Rs (autoreceptors) decreases the firing rate and serotonin secretion. In contrast, the activation of the post-synaptic receptor enhances the firing and secretion.[18,20] The administration of SSRIs results in a significant increase in extraneuronal serotonin that is quickly counteracted by a negative feedback mechanism mediated by autoreceptors; this in turn leads to the desensitization of the autoreceptors, but not of

[a] *Innovative Drug Research and Bioinformatics Group, School of Pharmaceutical Sciences and Collaborative Innovation Center for Brain Science, Chongqing University, Chongqing 401331, China. E-mail: xueww@cqu.edu.cn*
[b] *Innovative Drug Research and Bioinformatics Group, College of Pharmaceutical Sciences, Zhejiang University, Hangzhou, Zhejiang 310058, China. E-mail: zhufeng.ns@gmail.com, zhufeng@zju.edu.cn*
[c] *Bioinformatics and Drug Design Group, Department of Pharmacy, National University of Singapore, Singapore 117543, Singapore*
[d] *State Key Laboratory of Applied Organic Chemistry and Department of Chemistry, Lanzhou University, Lanzhou, 730000, China*
† Electronic supplementary information (ESI) available. See DOI: 10.1039/c7cp05688e

the post-synaptic receptors.[7,21] With the desensitization of the autoreceptors reduced, the autoreceptors gradually recover to release serotonin normally; thus, the greater activation of post-synaptic 5-HT_{1A} will relieve and improve the depression symptoms.[18,22] It was speculated that the delayed onset of action might result from the negative feedback mechanisms because it took time to recover the autoreceptors' normal serotonin release.[23–25] Thus, rapid desensitization of the autoreceptors is regarded as important in the fast onset of antidepressants,[25] which is proposed as a novel strategy for treating MDD.[26–28] In other words, a compound with the profile of both serotonin reuptake inhibition and 5-HT_{1A}R partial agonism (SPARI) has been expected to yield enhanced drug efficacy and rapid onset of action,[29–31] and consequently, substantial efforts have been made to discover new scaffolds of this mechanism.[32–36] To date, 2 SPARIs (vilazodone[37] and vortioxetine[38]) have been approved by the FDA for the treatment of MDD, and hundreds of active SPARIs of diverse scaffolds have been found *in vitro*.[24,30,32–34,39]

Vortioxetine showed multimodal activities by broadly binding to the serotonin reuptake transporter and 5-HT_{1A}, 5-HT_{1B}, 5-HT_3, 5-HT_7, and 5-HT_{1D} receptors.[40,41] Compared with vortioxetine, vilazodone and its analogues were much more selective to the serotonin transporter (SERT) and 5-HT_{1A}R[37,42] and thus capable of providing the most simplified and representative model of SPARIs' mechanism.[29] Moreover, due to the clinical importance of vilazodone, the binding mode of the privileged indolebutylpiperazine scaffold (residing in vilazodone and its analogues)[29] in SERT and 5-HT_{1A}R offered much more information about SPARIs' drug-like properties than that of the active SPARIs found *in vitro* and could facilitate the discovery of SPARI based on MDD drugs.[29,43]

On the one hand, the binding mode of 5-HT in SERT has already been revealed.[44] Due to the great structural similarity between 5-HT and the fragment indolebutylamine residing in vilazodone and its analogues, this fragment simulated 5-HT by competitively binding to SERT,[45–49] and the binding mode of vilazodone and its analogues in SERT could be effectively deduced.[44] On the other hand, to understand vilazodone's partial agonism to 5-HT_{1A}R and the resulting faster onset of action, it is very important to elucidate the binding mechanism of vilazodone and its analogues in 5-HT_{1A}R. However, this mechanism has not been reported to date; consequently, the discovery of novel and efficacious SPARI-based MDD drugs is severely hampered.

In this study, an integrated computational strategy was adopted to identify the binding mode of vilazodone and its analogues[29] in 5-HT_{1A}R. First, the structure of 5-HT_{1A}R was constructed by homology modelling based on the crystal structure of the β_2 adrenergic receptor (β_2AR).[50] Second, molecular docking combined with the Prime/MM-GBSA approach was applied to generate the binding poses of 51 ligands (vilazodone and its analogues) in the modelled target. Third, six representative ligand-target complexes were further selected and subjected to MD simulation and binding free energy analysis. As a result, a common binding mode shared by these six complexes was characterized by clustering 5-HT_{1A}R's residues in terms of their energy contribution to each ligand. Finally, an *in silico* alanine scanning mutagenesis study on these key residues contributing to drug binding was also performed to verify the reliability of the simulation results. Overall, the binding mechanism discovered herein can be regarded as a useful starting point for the design of novel chemical entities with improved antidepressant activity and pharmacological profiles.

Materials and methods

Sequence alignment and homology modelling

The sequence of human 5-HT_{1A}R was downloaded from the UniProt database (entry: P08990), and the sequence similarity search was conducted using the *SWISS-MODEL*[51] server. The disclosed co-crystal structure of β_2AR (PDB entry: 3SN6[50]) was selected as a template to build 5-HT_{1A}R. The sequence of human 5-HT_{1A}R was aligned with that of human β_2AR (PDB entry: 3SN6,[50] from E30 to C341) using *ClustalX 2.0*[52] and then visualized by *ESPript 3.0*.[53] The homology model of 5-HT_{1A}R was constructed using the automated mode of *SWISS-MODEL*[51] based on the template. Finally, the stereochemical quality of the modelled target was evaluated by Ramachandran plot analysis using *PROCHECK*.[54] The detailed protocol can be found in the ESI† for Materials and methods.

Molecular docking

The initial poses of the studied 51 ligands (Fig. 1) binding to the modelled 5-HT_{1A}R were obtained *via* standard precision (SP) docking in *Glide*[55] with the default settings. First, these 51 ligands were preprocessed by *LigPrep* using *OPLS-2005 force field*[56] to generate a low-energy conformation, and the ionized state was assigned by *Epik* at a pH value of 7.0 ± 2.0. The docking grid was calculated using the *Receptor Grid Generation* tool in *Glide*[50] by centering P0G (a ligand in 3SN6[50] introduced to the constructed 5-HT_{1A}R model) and simultaneously constraining an ionic bond interaction with the carboxylate of $D116^{3.32}$. The detailed protocol can be seen in the ESI† for Materials and methods.

Post-docking *via* prime optimization

The SP docking pose was submitted to optimization by *Prime*[57] followed by calculation of the binding free energy ($\Delta G_{\text{Prime/MM-GBSA}}$) *via* the following eqn (1):

$$\Delta G_{\text{Prime/MM-GBSA}} = \Delta E_{\text{MM}} + \Delta G_{\text{solv}} + \Delta G_{\text{SA}} \quad (1)$$

where ΔE_{MM} denotes the difference between the minimized energies of the docking complexes and the sum of the energy of the receptor and the ligand obtained using *OPLS-2005 force field*,[56] ΔG_{solv} is the difference between solvation energies of the complexes and the sum of solvation energies for the receptor and ligands obtained using the GBSA continuum model, and ΔG_{SA} indicates the difference between surface area energies of the complexes and the sum of surface area energies for the receptor and ligand.

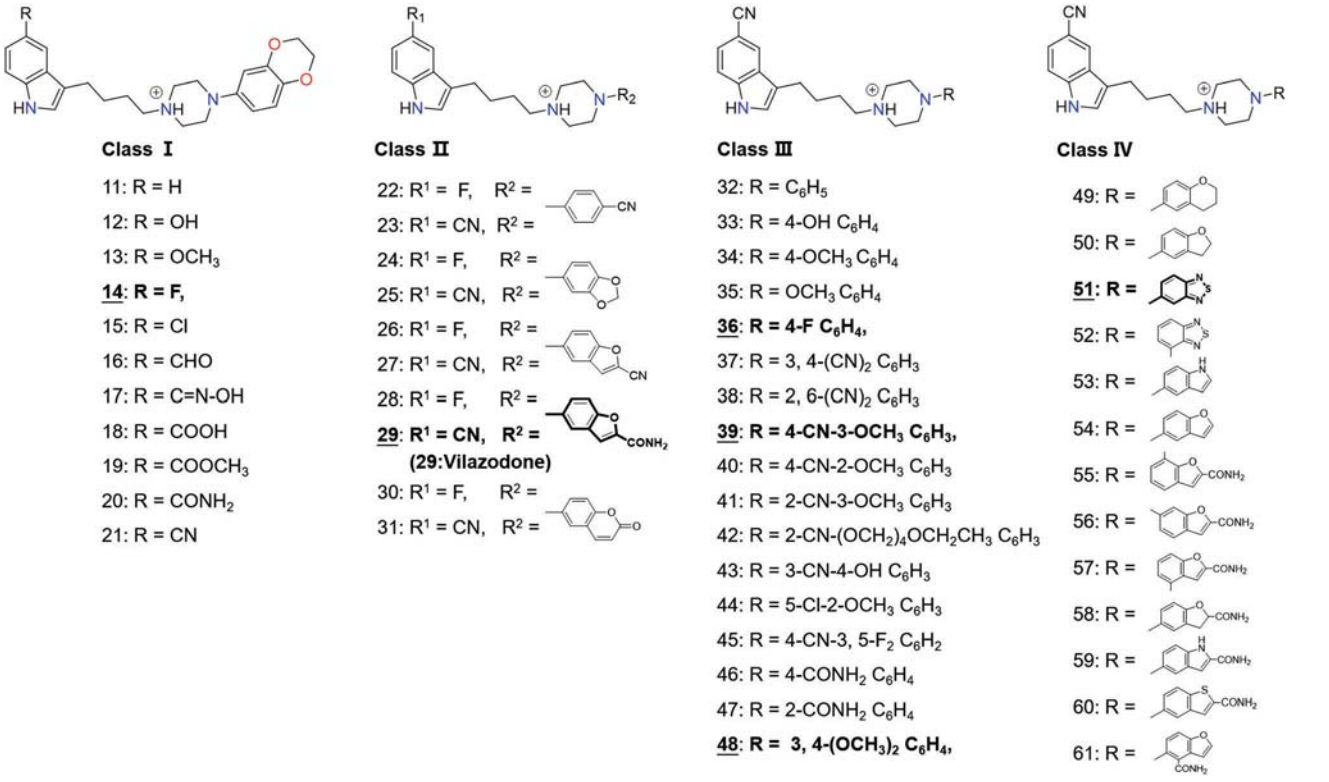

Fig. 1 Chemical structures of the studied 51 ligands.[29] These ligands were grouped into 4 classes with 6 representative ligands (**14**, **29**, **36**, **39**, **48**, and **51**, shown in bold) selected for the MD simulations. IC_{50} of these 6 ligands were 5.0 nM, 0.3 nM, 2.0 nM, 14.0 nM, 60.0 nM, and 2.0 nM.

MD simulation and binding free energy calculations

Preparing the MD simulation. Herein, 6 representative structures were selected from 51 receptor–ligand complexes for the MD simulations. Initially, the spatial orientations of these complexes were calculated by *OPM*[58] and then inserted into a POPC lipid bilayer with a water layer thickness of 20 Å and a NaCl concentration of 0.15 mol L^{-1} using *CHARMM-GUI Membrane Builder*.[59] Finally, the LEaP module in *AMBER14*[60] was used to assign the force field parameters for the protein (*ff14SB*[61]), lipid (*Lipid14*[62]), and water (*TIP3P*[63]). Ions (Na^+ and Cl^-) were modelled using parameters from Joung's work.[64] For the ligands, *Antechamber*[65] was adopted to assign *gaff*[66] atom types and *RESP*[67] partial atomic charges. The geometry optimization and the electrostatic potential calculation for the ligands were carried out using *Gaussian09* at the HF/6-31G* level. The size for each system was ~70 750 atoms, with the periodic box set as 80 Å × 80 Å × 113 Å.

Performing the MD simulations. MD simulations were performed with GPU-accelerated *PMEMD* in *AMBER14*.[60] Prior to the simulations, operational procedures (minimization, heating, and equilibration) were conducted, and the detailed protocol used herein is provided in the ESI,† Methods. Subsequently, 150 ns MD simulation was carried out in the *NPT* ensemble (310 K and 1 atm) under the periodic boundary condition. The *Particle-mesh Ewald algorithm*[68] was adopted to deal with the long-range electrostatic interaction (cut-off = 10 Å). The bond distance involving the bond to the hydrogen atom was constrained using the *SHAKE algorithm*,[69] and the integration time step was set as 2 fs in the simulations.

Calculating the binding free energy. The binding free energy ($\Delta G_{MM/GBSA}$) of the ligands to the receptor, excluding the entropic effect, was calculated by the MM/GBSA approach using a single trajectory. In this study, 500 images of the last 50 ns equilibrated trajectory were used. For each image, $\Delta G_{MM/GBSA}$ was computed as follows:

$$\Delta G_{MM/GBSA} = \Delta E_{vdW} + \Delta E_{ele} + \Delta G_{pol} + \Delta G_{nonpol} \quad (2)$$

where, ΔE_{vdW} denotes the van der Waals interaction energy, ΔE_{ele} stands for the electrostatic energy, ΔG_{pol} is the polar solvent interaction energy calculated *via* the GB model (*igb* = 2),[70] and ΔG_{nonpol} is the nonpolar solvation free energy, which has been evaluated as 0.0072 × ΔSASA using the LCPO method,[71] where SASA indicates the solvent accessible area determined with a probe radius of 1.4 Å.

Calculating the per-residue energy contribution. The per-residue energy contribution ($\Delta G^{per\text{-}residue}_{MM/GBSA}$) of the receptor to ligand binding was decomposed by the following equation:

$$\Delta G^{per\text{-}residue}_{MM/GBSA} = \Delta E^{per\text{-}residue}_{vdW} + \Delta E^{per\text{-}residue}_{ele} + \Delta G^{per\text{-}residue}_{pol} + \Delta G^{per\text{-}residue}_{nonpol} \quad (3)$$

where the way to define $\Delta E^{per\text{-}residue}_{vdW}$, $\Delta E^{per\text{-}residue}_{ele}$, and $\Delta G^{per\text{-}residue}_{pol}$ was the same as that in eqn (2), but the nonpolar solvent interaction energy ($\Delta G^{per\text{-}residue}_{nonpol}$) was calculated by a

recursive approximation of a sphere around an atom starting from an icosahedron (ICOSA).

Hierarchical clustering

Hierarchical clustering was performed by the *R* statistical analysis software.[72] At first, a 6-dimensional vector was generated by the energy contributions of a certain residue to at least one ligand binding ($\neq$ 0 kcal mol^{-1}), and the similarity among the vectors was then calculated in terms of the *Manhattan* distance:

$$\text{Distance}(a,b) = \sum_i |a_i - b_i| \quad (4)$$

where i indicates the dimension of the energy contribution of the residues a and b. The *Ward's minimum variance* algorithm[73] was used to minimize the total within-cluster variance. Finally, the cluster outcomes were displayed using the web-server named *iTOL*.[74]

Computational alanine scanning mutagenesis

Computational alanine scanning (CAS) is acknowledged as an effective approach[75] for identifying hot spots at the binding sites[76,77] of protein–protein, protein–DNA, and protein–ligand interactions. Herein, CAS was conducted to verify the identified key residues contributing to the binding. For alanine mutation, the variation of the binding free energies between the mutant and wild-type was defined as follows:

$$\Delta G_{\text{mutant/wild-type}} = \Delta G_{\text{mutant}} - \Delta G_{\text{wild-type}} \quad (5)$$

where ΔG_{mutant} and $\Delta G_{\text{wild-type}}$ were calculated from 500 images extracted from the MD simulations. The alanine mutation was generated by truncating the side chain of mutated residues at C_γ and replacing this with a hydrogen atom (C_β–H).[76] The alanine scanning conducted herein was applied only to the selected residues with a high absolute binding energy contribution ($>$0.50 kcal mol^{-1}).[77]

Results and discussion

Homology model of 5-HT$_{1A}$R in an agonistic conformation

The construction of the correct binding pocket conformation has been reported to be critical for the rational design of drugs targeting GPCR.[78] The ligands studied herein act as partial agonists of 5-HT$_{1A}$R,[29] and the active state crystal structure of an agonist-stabilized β_2AR (in an agonistic conformation, PDB entry: 3SN6[50]) has already been adopted as a template for constructing the homology models of 5-HT$_{1A}$R in several virtual screening studies.[79–81] Therefore, the agonist-stabilized β_2AR 3SN6 was selected herein as the template for the homology modelling. The sequence alignment between the target and template (ESI,† Fig. S1) revealed an overall residue identity of 34% and a binding pocket residue conservation of 41%. The binding pocket in the modelled receptor was identified by the interaction between P0G and β_2AR and surrounded by the residues in the vicinity of the ligand ($<$6 Å, ESI,† Fig. S2). As shown in ESI,† Fig. S3, the homology model constructed in this study was superimposed well with its template. As expected, this model adopted a conformation similar to that of the active state β_2AR that covered the transmembrane helices (TM1-7) associated with the intracellular (LCL) and extracellular (ECL) loop regions (ESI,† Fig. S3). Moreover, the overall quality of the constructed model was evaluated by the Ramachandran plot analysis. As shown in ESI,† Fig. S4, the majority (98.5%) of the residues were located in the allowed regions. Therefore, the modelled 5-HT$_{1A}$R in the agonistic conformation was qualified enough to study its interactions with vilazodone and its analogues.

Docking of the ligands into 5-HT$_{1A}$R

A total of 51 ligands[29] (Fig. 1) were studied herein. According to their diverse structural features, these ligands (**11** to **61**, with their original ligand ID retained[29]) were grouped into four classes: (I) **11–21**, (II) **22–31**, (III) **32–48**, and (IV) **49–61**, in a similar way as that reported in Heinrich's work[29] (ESI,† Tables S1–S4), and vilazodone was numbered as ligand **29**. At first, these 51 ligands were docked into the binding pocket to obtain the initial receptor–ligand complexes and then subjected to post-processing optimization. The post-processed docking poses of these 51 ligands are depicted by classes in Fig. 2. As illustrated, the positively charged ammonium moiety of all 51 ligands directly interacted with the carboxylate of D116$^{3.32}$ *via* a salt bridge, and the ligands' indole formed a hydrogen bond with S199$^{5.42}$. The salt bridge represented conserved protein–ligand recognition (anchor site) throughout a wide range of mammalian biogenic amine GPCRs,[38,80] and the hydrogen bond was found to be essential for the agonism of these partial agonists[82] studied herein.

The post-docking scores ($\Delta G_{\text{Prime/MM-GBSA}}$) of all 51 complexes are listed in Table S5 (ESI†). The correlation coefficient R^2 between ΔG_{exp} (binding energy deduced from the experimental data[29]) and ΔG_{bind} was 0.84 (Fig. 3). This high correlation was in accordance with the previous studies stating that molecular docking combined with the Prime/MM-GBSA approach enabled a rapid estimation of the binding affinity of a series of ligands to their corresponding receptor.[83–87] Moreover, two outliers (ligands **17** and **18** shown in Fig. 3) have also been observed, which may have originated from the unfavorable contribution of their substituents on indole at position 5 to their binding to 5-HT$_{1A}$R. In particular, as shown in ESI,† Fig. S5, a strong polar group (−C═NOH and –COOH circled by red dash line) was orientated into the hydrophobic cavity between TM6 and TM7 constituted by 13 hydrophobic residues (F361$^{6.51}$, F362$^{6.52}$, I363$^{6.53}$, V364$^{6.54}$, A365$^{6.55}$, L366$^{6.56}$, V367$^{6.57}$, L380$^{7.32}$, L381$^{7.33}$, G382$^{7.34}$, A383$^{7.35}$, I384$^{7.36}$, and I385$^{7.37}$). The hydrophobic region may repel these polar moieties and hence may not stabilize the ligands in the binding pocket. Thus, the local region did not favor the binding of these two ligands with 5-HT$_{1A}$R.

MD simulations and binding free energy calculations of the receptor–ligand complexes

MD simulation can be used as a post-processing tool for validating or refining docking solutions. To explore more detailed and reliable information on the binding mode, 6 representative

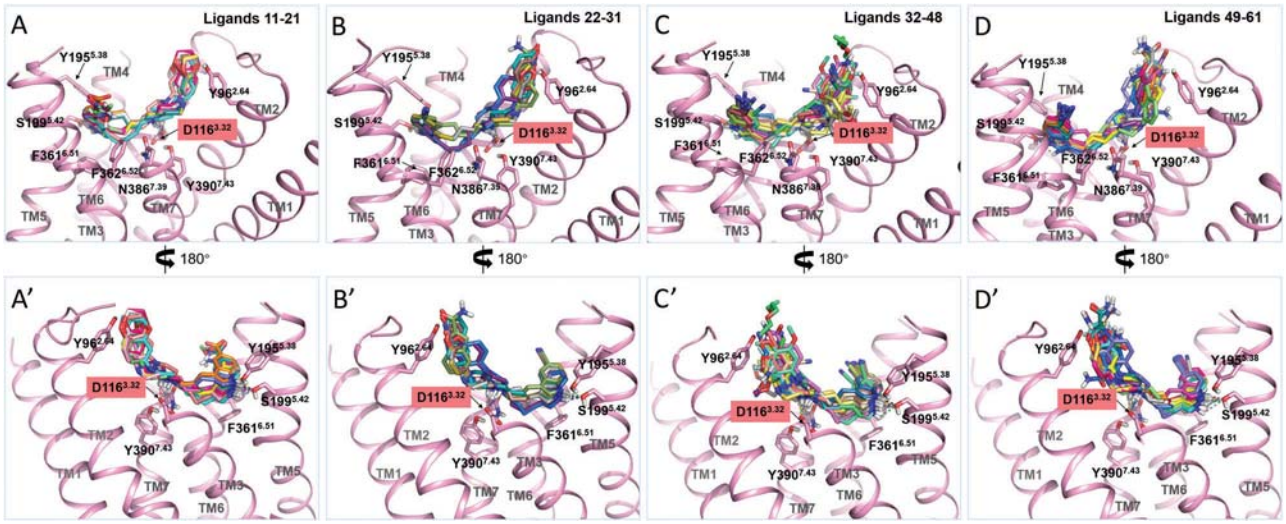

Fig. 2 The post-docking poses of 4 classes of vilazodone and its analogues in the binding pocket of the human 5-HT_{1A} receptor. Receptors are displayed in pink cartoons and the residues in the orthostatic binding pocket are shown as pink sticks. Ligands are shown by various colors. Residues labeled in red background represent the ionic bond interactions existing between the ligands and receptor.

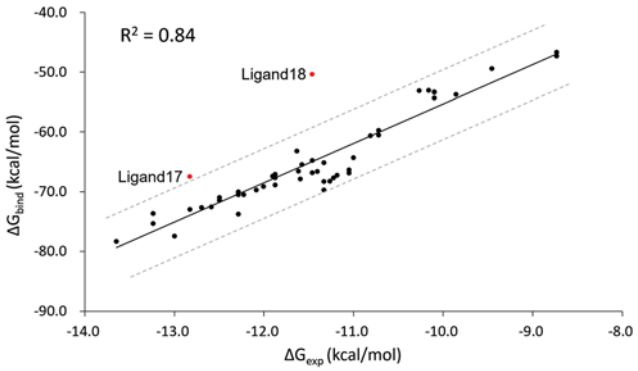

Fig. 3 Correlation between the experimentally determined binding free energy (ΔG_{exp}) and post-docking binding energy (ΔG_{bind}) obtained by Prime/MM-GBSA.

Table 1 The calculated and experimentally determined binding free energies throughout 6 complexes (ΔG is in kcal mol^{-1} and IC_{50} is in nM)

Ligands	$\Delta G_{MM/GBSA}$	$\Delta\Delta G_{calc}$ [a]	ΔG_{exp} [b]	$\Delta\Delta G_{exp}$	IC_{50} [c]
29	−62.73	−11.08	−13.00	−3.14	0.30
36	−59.63	−7.98	−11.87	−2.01	2.00
51	−58.10	−6.45	−11.87	−2.01	2.00
14	−57.29	−5.64	−11.33	−1.47	5.00
39	−56.17	−4.52	−10.72	−0.86	14.00
48	−51.65	0.00	−9.86	0.00	60.00

[a] $\Delta\Delta G$ denotes the difference in binding energies (ΔG) using ligand **48** as a reference. [b] Estimated free energy values are computed by $\Delta G_{exp} = RT\ln IC_{50}$ based on IC_{50} values. [c] Experimental IC_{50} values from the previous study.[29]

complexes from the docking study were selected and subjected to MD simulations followed by binding energy calculations. The selected ligands included **14** from class I, **29** (vilazodone) from class II, **36**, **39**, and **48** from class III, and **51** from class IV, whose binding affinities to 5-HT_{1A}R ranged from 0.3 nM to 60.0 nM (Table 1).

Simulation stability evaluation. The root-mean-square deviation (RMSD) of protein backbone atoms, ligand heavy atoms, and binding site residues atoms (extending 6 Å around the ligand) for 6 simulation systems against the simulation time was calculated, and the results are illustrated in ESI,† Fig. S6. These RMSD values (fluctuation range within 4 Å) manifested that all systems achieved their equilibrium state after 100 ns simulation. Moreover, the salt bridge between the positively charged nitrogen of all the ligands and the carboxyl of $D116^{3.32}$ in the receptor[88] was analyzed by superimposing the initial docking poses with the MD simulation results (ESI,† Fig. S7). It was noted that although there was a certain level of structural shifts on both the target and ligands, the conserved salt bridges were maintained very well during the whole MD simulation.

Binding free energy calculations. The free energy of binding ($\Delta G_{MM/GBSA}$) of vilazodone and its analogues to 5-HT_{1A}R was quantitatively calculated by the MM/GBSA method. As shown in Table 1, the calculated $\Delta G_{MM/GBSA}$ corresponding to **29**, **36**, **51**, **14**, **39**, and **48** bound complexes was −62.73, −59.63, −58.10, −57.29, −56.17, and −51.65 kcal mol^{-1}, respectively. Moreover, the binding free energies of these 6 complexes could be deduced by experiment. In particular, the experimental IC_{50} values[29] could be converted into binding energies (ΔG_{exp}) using the equation $\Delta G_{exp} = RT\ln(IC_{50})$, and the resulting binding energies (ΔG_{exp}) were −13.00, −11.87, −11.87, −11.33, −10.72, and −9.86 kcal mol^{-1}. Using ligand **48** as a reference, the differences between binding energy ($\Delta\Delta G$) of the studied ligands and **48** were used to estimate the reproducibility of the experimental results by the simulations.[45,89] As shown in Fig. 4, the simulation results of this study ($\Delta\Delta G_{MM/GBSA}$) rendered a good correlation (R^2 = 0.95) with the experimental results ($\Delta\Delta G_{exp}$), but an overestimation by simulation was observed (Table 1). As reported, if only the relative order of the binding affinity of ligands with a similar structure and

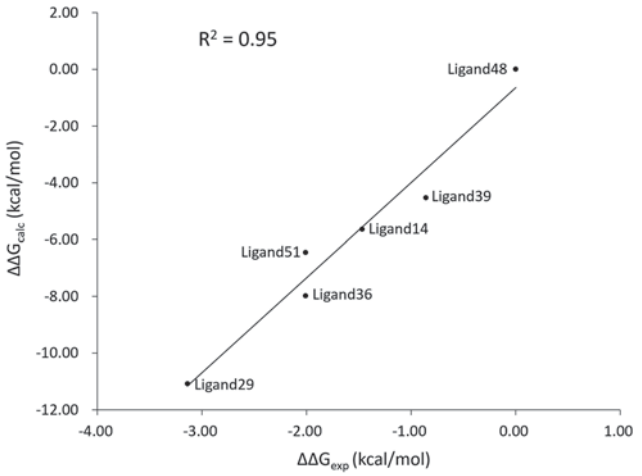

Fig. 4 Correlation between the differences in the calculated ($\Delta\Delta G_{calc}$) and experimentally determined ($\Delta\Delta G_{exp}$) binding free energies using ligand **48** as the reference.

resembled binding conformation was taken into consideration, the entropy contribution could be ignored,[45,89,90] and the above-mentioned overestimation was inevitable, as shown in the literature using the MM/GBSA method.[91–94] In Table S6 (ESI†), values for the detailed energy terms shown in eqn (1) are provided. As shown, the van der Waals (ΔE_{vdW}), the electrostatic interaction (ΔE_{ele}), and the nonpolar solvation (ΔG_{nonpol}) terms were favorable for the ligands' binding, whereas the polar solvation component ΔG_{pol} was unfavorable. Among these favorable terms, ΔE_{vdW} accounted for the major part of the energy contributions for all 6 studied complexes, with the ligand **29**-bound complex being at the top rank ($\Delta E_{vdW} = -58.41$ kcal mol^{-1}) and the ligand **48**-bound complex being at the lowest rank ($\Delta E_{vdW} = -50.10$ kcal mol^{-1}). The lowest ΔE_{vdW} of ligand **48** might originate from the two electron-donating groups ($-OCH_3$) on its aromatic ring of arylpiperazine, which enhanced the electron density of the ring and in turn hampered the binding of ligand **48** to the binding pocket of 5-HT$_{1A}$R.

Comprehensive analysis of the receptor–ligand interactions

Fig. 5 shows the 6 representative images obtained from the MD simulations of the receptor–ligand complexes. The detailed binding mode of each ligand is described in the ESI† for Results and discussion. In this section, the receptor–ligand interactions are systematically analyzed from four different perspectives: first, the residues in the vicinity of the studied

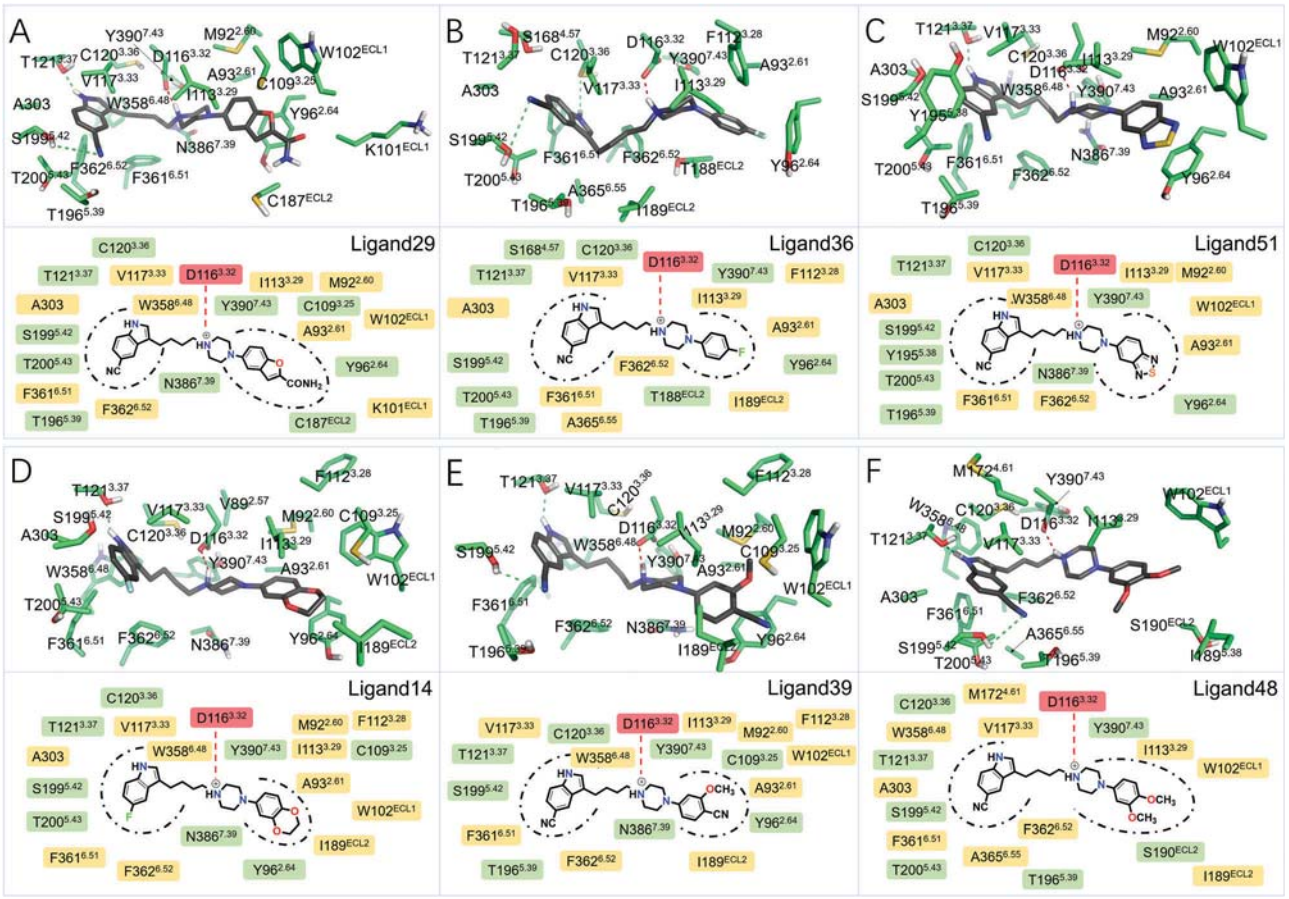

Fig. 5 The representative images of 6 ligands (dark sticks) with residues (green sticks) in the binding pocket of the 5-HT$_{1A}$ receptor. Residues labeled in red, yellow, and green backgrounds represent the ionic bonds, hydrophobic interactions, and polar interactions existing between the residues and ligands, and the ionic bridges and hydrogen bonds are shown by the red dashed lines and green dashed lines, respectively.

ligands are discussed based on the MD simulations; second, the key residues making a high contribution to the ligands' binding are identified by the per-residue energy decomposition; third, the hotspots consistently contributing to the binding of all the studied ligands are discovered by hierarchical clustering analysis; and finally, these identified hotspots are further validated by computational alanine scanning.

Polar and nonpolar residues in the vicinity of the studied ligands. Fig. 5 shows the representative snapshots of the 6 receptor–ligand complexes. The detailed binding modes of all the ligands are provided in the ESI† for Results and discussion. As shown, the studied ligands interacted with 9 residues in their close vicinity (<6 Å), including 5 polar (D116$^{3.32}$, C120$^{3.36}$, T121$^{3.37}$, S199$^{5.42}$, and Y390$^{7.43}$) and 4 nonpolar (I113$^{3.29}$, V117$^{3.33}$, F361$^{6.51}$, and F362$^{6.52}$) residues.

Ionic (salt bridge) interaction was preserved between the positively charged nitrogen of the studied ligand and the carboxyl oxygen on D116$^{3.32}$ of the receptor (Fig. 5), which was validated by the previous site-directed mutagenesis experiment.[95] Moreover, −OH of Y390$^{7.43}$ formed a hydrogen bond with the charged center of each ligand. As known, these abovementioned polar interactions could result in an enthalpy gain, which in turn drove the ligands' binding in 5-HT$_{1A}$R.[45,89,96–98] Moreover, the hydrogen atom attached to nitrogen in the indole ring of each ligand formed a hydrogen bond with either T121$^{3.37}$ or C120$^{3.36}$ (both with a polar side chain). In addition, polar-substituted groups with an electron-withdrawing profile (−F or −CN) at the 5-position of indole rings formed a hydrogen bond with the −OH of S199$^{5.42}$, which were, therefore, speculated to facilitate the ligands' binding.[99]

As illustrated in Fig. 5, I113$^{3.29}$, V117$^{3.33}$, F361$^{6.51}$, and F362$^{6.52}$ made hydrophobic interactions with all the studied ligands *via* their nonpolar side chain. The side chains of F361$^{6.51}$ and F362$^{6.52}$ were below the distal indole ring of the ligand and almost perpendicular (83–89°) to the plane of the ligand's heterocyclic ring, thereby fostering edge-to-face π–π interactions between the residues and ligands. Different from F361$^{6.51}$ and F362$^{6.52}$, V117$^{3.33}$ resided above the plane of the ligand's indole ring. I113$^{3.29}$ in the vicinity of the arylpiperazine moiety stabilized the aromatic ring *via* the −CH–π interaction. As shown in Fig. 5, all these residues were located on TM3, TM5, TM6, and TM7 and played essential roles in stabilizing ligand binding *via* the hydrophobic interactions to 5-HT$_{1A}$R.

Key residues making a high energy contribution to the ligands' binding. To identify the key residues contributing to the binding of vilazodone and its analogues, the total energy was projected to each residue of 5-HT$_{1A}$R. As illustrated in Fig. 6, the 21, 19, 19, 21, 19, and 19 residues with a high absolute energy contribution (>0.5 kcal mol^{-1}) were identified to favor the binding of the ligands **29**, **36**, **51**, **14**, **39**, and **48**, respectively. On the one hand, the energy contribution of different residues to the same ligand varied significantly. For example, Y96$^{2.64}$ made one of the highest contribution (−3.03 kcal mol^{-1}) to the binding of **29**, whereas A93$^{2.61}$ made one of the lowest contribution (−0.55 kcal mol^{-1}). On the other hand, the contributions of the same residue to various ligands also differed greatly. For instance, the energy contributions of D116$^{3.32}$ to the binding of **14** and **48** were −1.33 and −0.42 kcal mol^{-1}, respectively. Moreover, the energy contributions of the 9 residues (I113$^{3.29}$, D116$^{3.32}$, V117$^{3.33}$, C120$^{3.36}$, T121$^{3.37}$, S199$^{5.42}$, F361$^{6.51}$, F362$^{6.52}$, and Y390$^{7.43}$), as discussed in the previous section, in the vicinity of the studied ligands were larger than −0.50 kcal mol^{-1}, and 10 residues (M92$^{2.60}$, A93$^{2.61}$, Y96$^{2.64}$, W102^{ECL1}, I189^{ECL2}, T196$^{5.39}$, T200$^{5.43}$, A303, W358$^{6.48}$, and N386$^{7.39}$) were discovered to favor the binding of at least 4 ligands (|energy contribution| > 0.5 kcal mol^{-1}).

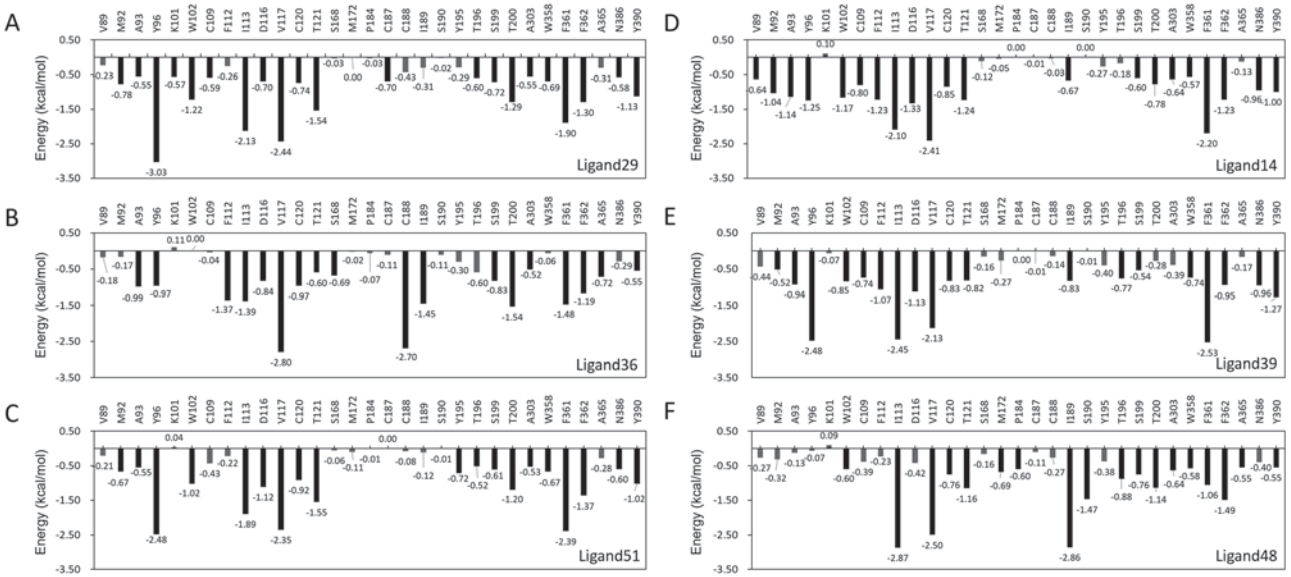

Fig. 6 Per-residue binding energy decomposition of 6 ligands complexed with the 5-HT$_{1A}$ receptor. A union set of residues with an energy contribution (the absolute value) larger than 0.50 kcal mol^{-1} to at least one studied ligand are displayed. Black and grey bars indicate the energy contributions larger and lower than 0.50 kcal mol^{-1}, respectively.

Identification of hotspots consistently favoring the ligands' binding. Per-residue energy contribution decomposition analysis indicated that there were common features for the binding of all the ligands to human 5-HT_{1A}R. To characterize the key residues consistently favorable for the 6 ligands' binding, hierarchical clustering analysis was employed to categorize the residues in terms of their energy contributions. As shown in Fig. 7, the residues in *cluster A* contributed much higher than other residues to the binding of all the ligands, which could be further grouped into *cluster* A_1 and *cluster* A_2 based on the clustering results. In total, the residues in *cluster A* provided 61.18%, 69.01%, 63.32%, 67.87%, 62.88%, and 63.73% contributions to the binding of **29**, **36**, **51**, **14**, **39**, and **48**, respectively. Among these, the energy contributions offered by the residues in *cluster* A_1 to the binding of ligands **29**, **36**, **51**, **14**, **39**, and **48** amounted to 39.48%, 29.23%, 40.85%, 33.13%, 41.30%, and 28.89%, respectively.

Moreover, as shown in Fig. 6, $T188^{ECL2}$ contributed -2.70 kcal mol^{-1} energy to the binding of **36**, but much less energy to the others. $W102^{ECL1}$, $M92^{2.60}$, $N386^{7.39}$, $C109^{3.25}$, and $W358^{6.48}$ contributed to the binding of **36** by -0.56 kcal mol^{-1} in total. From the tree cluster, it was apparent that the energy of $T188^{ECL2}$ might compensate the lower energy originating from $W102^{ECL1}$, $M92^{2.60}$, $N386^{7.39}$, $C109^{3.25}$, and $W358^{6.48}$ (as shown in Fig. 6D and 7). $Y96^{2.64}$ contributed much less to the binding of **48** (-0.07 kcal mol^{-1}), whereas the contribution of $I189^{ECL2}$ (-2.86 kcal mol^{-1}) might compensate the lower energy offered by $Y96^{2.64}$ (as shown in Fig. 6F and 7).

Verification of the identified hotspots by computational alanine scanning. As shown in Fig. 7, 22 hotspots were identified and could be further verified by computational alanine scanning. As shown in Fig. S8 (ESI†), the energy differences ($\Delta\Delta G_{mut-wild}$) of all the mutated residues were positive; this indicated that these alanine mutations disfavored the ligands' binding. The $\Delta\Delta G_{mut-wild}$ values of the residues in *cluster* A_1 and *cluster* A_2 are displayed in Fig. S8A and S8B–E, respectively. Generally, the more positive $\Delta\Delta G_{mut-wild}$ indicated the more importance in terms of the corresponding residue for ligands' binding. The binding free energies for all 6 ligands dropped dramatically when the residues in *cluster* A_1 were mutated to

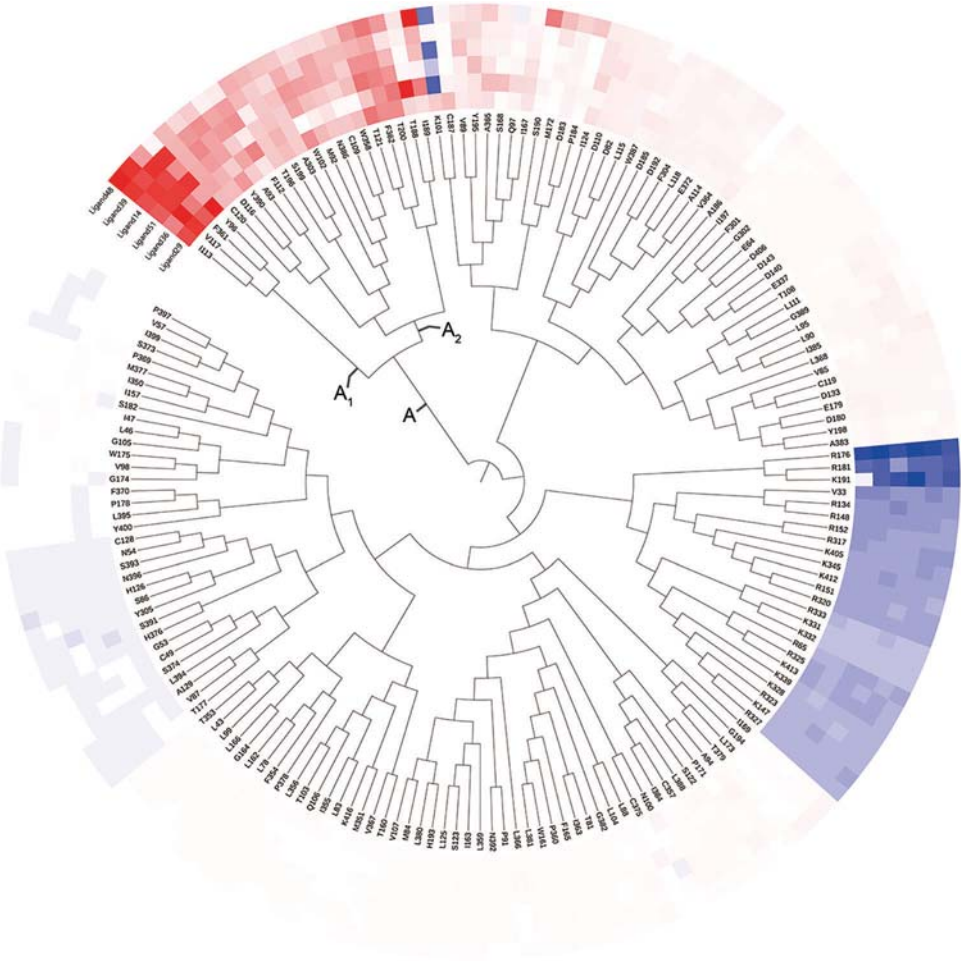

Fig. 7 Tree cluster of 178 residues with an energy contribution ($\neq$ 0 kcal mol^{-1}) to at least one ligand. Per-residue binding energy contributions favoring ligand's binding are displayed in red, with the highest contribution set as exact red and lower ones gradually fading toward white (no contribution). Per-residue energy contributions hampering ligand's binding are shown in blue, with the highest contribution set as exact blue and lower contribution set gradually fading towards white.

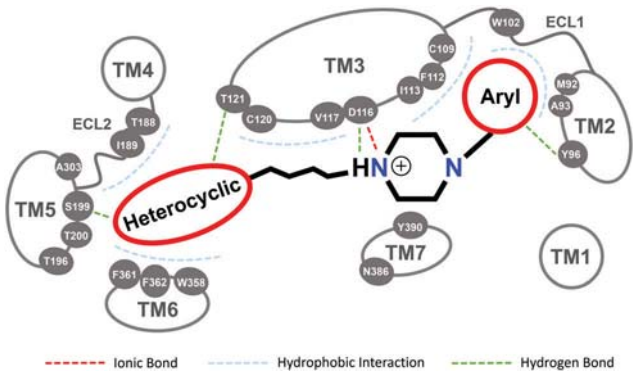

Fig. 8 Schematic of the binding mode of vilazodone and its analogues to the 5-HT_{1A} receptor. TM1-7 and ECL indicate the seven transmembrane and extracellular regions, respectively. The location of the residues and interaction types between the residues and ligands are depicted. Red, light blue, and green dashed lines refer to the ionic bonds, hydrophobic interactions, and hydrogen bonds, respectively. The aryl moiety and heterocyclic ring moiety and linker are highlighted in red and black, respectively.

alanine. For ligand **36**, the mutation of $Y96^{2.64}$ and $I113^{3.29}$ to alanine had a subtle effect ($\Delta\Delta G_{mut-wild}$ = 0.97 kcal mol^{-1}) on the binding free energy (Fig. S8A, ESI†), but the alanine mutation of $F112^{3.28}$ (Fig. S8D, ESI†) exerted obvious impacts on the binding of **36**. Compared to the residues in *cluster* A_1, $D116^{3.32}$ in *cluster* A_2 was also essential for the ligands' binding due to the large variations ($\Delta\Delta G_{mut-wild} > 3.0$ kcal mol^{-1}) resulted from the alanine mutation. In particular, the mutation $D116^{3.32}$ to alanine for the ligand **51**-bound complex resulted in the largest change ($\Delta\Delta G_{mut-wild}$ = 5.98 kcal mol^{-1}); this demonstrated that $D116^{3.32}$ as a recognition site played a paramount role in the ligands' binding (Fig. S8B, ESI†). $Y390^{7.43}$ and $F362^{6.52}$ also produced great effects on the binding of the 6 ligands. Mutations of their aromatic rings to a small side chain ($-CH_3$) decreased the hydrophobic interactions between the ligands and 5-HT_{1A}R, thereby reflecting the significant role of this interaction in the ligands' binding. $F362^{6.52}$ mutation resulted in a little change in the binding energy for ligand **39** ($\Delta\Delta G_{mut-wild}$ = 0.17 kcal mol^{-1}). There might be no interactions between indole and phenyl of $F362^{6.52}$ in the **39** complex due to the long interaction distance (>4.5 Å) (Fig. 5E). The mutation of $N386^{7.39}$ caused <2.0 kcal mol^{-1} energy change (Fig. 7B), but had modest effects on the binding free energy of all the ligands. These results showed the significance of $N386^{7.39}$ in the ligand–receptor interaction, and alanine scanning mutation converted the polar side chain to a nonpolar side chain with the polar interactions between ligands and receptor decreased.

Discovering the inhibitory mechanism of vilazodone and its analogues

As illustrated in Fig. 8, 22 hotspots identified in this study were primarily mapped to TM2, TM3, TM5, TM6, TM7, ECL1, and ECL2. Among these hotspots, some (such as $D116^{3.32}$ and $N386^{7.39}$) had also been discovered in site-directed mutagenesis studies,[39,79,100–103] and all were located in the general orthostatic binding pocket in GPCR.[80,104,105] In this study, three main interactions between vilazodone's analogues and 5-HT_{1A}R were identified and are schematically represented in Fig. 8. These have been described as follows: (1) salt bridges and polar interactions with the piperazine group of vilazodone and its analogues. In particular, carboxyl of $D116^{3.32}$ recognized vilazodone's analogues *via* a salt bridge, and two residues ($N386^{7.39}$ and $Y390^{7.43}$) stabilized the positively charged center of these analogues *via* polar interactions; (2) hydrogen bonds and hydrophobic interactions with the indole ring moiety of vilazodone and its analogues. In particular, the indole ring moiety engaged in hydrogen bonds with $T121^{3.37}$, $C120^{3.36}$ and $S199^{5.42}$, and the residues ($V117^{3.33}$, $T188^{ECL2}$, $I189^{ECL2}$, $T196^{5.39}$, $S199^{5.42}$, $T200^{5.43}$, A303, $W358^{6.48}$, $F361^{6.51}$, and $F362^{6.52}$) around it provided energies to the binding of vilazodone's analogues *via* hydrophobic interactions; (3) hydrophobic interactions and hydrogen bonds with the polar group on the arylpiperazine ring of vilazodone and its analogues. $Y96^{2.64}$ formed a hydrogen bond with the ligands' polar group on their arylpiperazine ring, and 5 residues ($M92^{2.60}$, $A93^{2.61}$, $W102^{ECL1}$, $F112^{3.28}$, and $I113^{3.29}$) stabilized the ligands *via* hydrophobic interactions.

The agonism of vilazodone and its analogues to 5-HT_{1A}R, as shown in Fig. 8, will provide substantial information to medicinal chemists working in the field of rational design of novel SPARIs for MDD treatment. First, polar or hydrophilic groups substituted in the aryl moiety need to point into 5-HT_{1A}R's polar extracellular region. Second, a heterocyclic moiety structurally similar to 5-HT[29] with the electron-withdrawing group could increase SPARIs' binding affinity to 5-HT_{1A}R. Third, the polar group on the butyl linker could enhance SPARIs' interaction with some residues ($N386^{7.39}$ and $Y390^{7.43}$) in 5-HT_{1A}R. Fourth, the strategy of balancing the arylpiperazine ring and heterocyclic moiety in target recognition could provide insights into the design of highly active SPARIs when binding to 5-HT_{1A}R.

Conclusion

The binding mechanism underlying the partial agonism of vilazodone and its analogues to 5-HT_{1A}R was revealed in this study using an integrated computational strategy. Herein, 22 residues of 5-HT_{1A}R were identified as hotspots, consistently favoring the binding of vilazodone and its analogues, and a common binding mode underlying their partial agonism to 5-HT_{1A}R was, therefore, discovered. Moreover, three main interaction features between vilazodone and 5-HT_{1A}R were revealed and have been schematically summarized. This identified binding mechanism underlying the partial agonism of vilazodone and its analogues to 5-HT_{1A}R will provide substantial insights into the design of highly efficacious SPARIs while binding to 5-HT_{1A}R.

Conflicts of interest

There are no conflicts to declare.

Acknowledgements

This work was supported by the Precision Medicine Project of the National Key Research and Development Plan of China (2016YFC0902200), the National Natural Science Foundation of China (21505009), the Innovation Project on Industrial Generic Key Technologies of Chongqing (cstc2015zdcy-ztzx120003), and the Fundamental Research Funds for Central Universities (10611CDJXZ238826, CDJZR14468801, CDJKXB14011).

References

1 C. Global Burden of Disease Study, *Lancet*, 2015, **386**, 743–800.
2 G. E. Hodes, V. Kana, C. Menard, M. Merad and S. J. Russo, *Nat. Neurosci.*, 2015, **18**, 1386–1393.
3 H. Yang, C. Qin, Y. H. Li, L. Tao, J. Zhou, C. Y. Yu, F. Xu, Z. Chen, F. Zhu and Y. Z. Chen, *Nucleic Acids Res.*, 2016, **44**, D1069–1074.
4 G. Yang, Y. Wang, Y. Zeng, G. F. Gao, X. Liang, M. Zhou, X. Wan, S. Yu, Y. Jiang, M. Naghavi, T. Vos, H. Wang, A. D. Lopez and C. J. Murray, *Lancet*, 2013, **381**, 1987–2015.
5 M. J. Ramaker and S. C. Dulawa, *Mol. Psychiatry*, 2017, **22**, 656–665.
6 Y. H. Li, P. P. Wang, X. X. Li, C. Y. Yu, H. Yang, J. Zhou, W. W. Xue, J. Tan and F. Zhu, *PLoS One*, 2016, **11**, e0165737.
7 X. Cai, A. J. Kallarackal, M. D. Kvarta, S. Goluskin, K. Gaylor, A. M. Bailey, H. K. Lee, R. L. Huganir and S. M. Thompson, *Nat. Neurosci.*, 2013, **16**, 464–472.
8 F. Zhu, B. Han, P. Kumar, X. Liu, X. Ma, X. Wei, L. Huang, Y. Guo, L. Han, C. Zheng and Y. Chen, *Nucleic Acids Res.*, 2010, **38**, D787–791.
9 F. Zhu, Z. Shi, C. Qin, L. Tao, X. Liu, F. Xu, L. Zhang, Y. Song, X. Liu, J. Zhang, B. Han, P. Zhang and Y. Chen, *Nucleic Acids Res.*, 2012, **40**, D1128–1136.
10 A. Cipriani, X. Zhou, C. Del Giovane, S. E. Hetrick, B. Qin, C. Whittington, D. Coghill, Y. Zhang, P. Hazell, S. Leucht, P. Cuijpers, J. Pu, D. Cohen, A. V. Ravindran, Y. Liu, K. D. Michael, L. Yang, L. Liu and P. Xie, *Lancet*, 2016, **388**, 881–890.
11 V. M. Castro, C. C. Clements, S. N. Murphy, V. S. Gainer, M. Fava, J. B. Weilburg, J. L. Erb, S. E. Churchill, I. S. Kohane, D. V. Iosifescu, J. W. Smoller and R. H. Perlis, *BMJ*, 2013, **346**, f288.
12 P. Wang, X. Zhang, T. Fu, S. Li, B. Li, W. Xue, X. Yao, Y. Chen and F. Zhu, *ACS Chem. Neurosci.*, 2017, **8**, 1416–1428.
13 P. Wang, T. Fu, X. Zhang, F. Yang, G. Zheng, W. Xue, Y. Chen, X. Yao and F. Zhu, *Biochim. Biophys. Acta, Gen. Subj.*, 2017, **1861**, 2766–2777.
14 G. I. Papakostas, M. E. Thase, M. Fava, J. C. Nelson and R. C. Shelton, *Biol. Psychiatry*, 2007, **62**, 1217–1227.
15 S. M. Huang, A. Bhattaram, N. Mehrotra and Y. Wang, *Clin. Pharmacol. Ther.*, 2013, **93**, 159–162.
16 D. Spinks and G. Spinks, *Curr. Med. Chem.*, 2002, **9**, 799–810.
17 P. Pacher, E. Kohegyi, V. Kecskemeti and S. Furst, *Curr. Med. Chem.*, 2001, **8**, 89–100.
18 P. Celada, A. Bortolozzi and F. Artigas, *CNS Drugs*, 2013, **27**, 703–716.
19 F. Artigas, *Pharmacol. Ther.*, 2013, **137**, 119–131.
20 K. Immadisetty, L. M. Geffert, C. K. Surratt and J. D. Madura, *Expert Opin. Drug Discovery*, 2013, **8**, 1399–1414.
21 S. M. Wang, C. Han, S. J. Lee, A. A. Patkar, P. S. Masand and C. U. Pae, *Chonnam Med. J.*, 2016, **52**, 91–100.
22 C. N. Yohn, M. M. Gergues and B. A. Samuels, *Mol. Brain*, 2017, **10**, 28–39.
23 N. Haddjeri, C. Ortemann, C. de Montigny and P. Blier, *Eur. Neuropsychopharmacol.*, 1999, **9**, 427–440.
24 Y. H. Li, J. Y. Xu, L. Tao, X. F. Li, S. Li, X. Zeng, S. Y. Chen, P. Zhang, C. Qin, C. Zhang, Z. Chen, F. Zhu and Y. Z. Chen, *PLoS One*, 2016, **11**, e0155290.
25 P. Celada, M. Puig, M. Amargos-Bosch, A. Adell and F. Artigas, *J. Psychiatry. Neurosci.*, 2004, **29**, 252–265.
26 S. Bollinger, H. Hubner, F. W. Heinemann, K. Meyer and P. Gmeiner, *J. Med. Chem.*, 2010, **53**, 7167–7179.
27 L. Tao, F. Zhu, F. Xu, Z. Chen, Y. Y. Jiang and Y. Z. Chen, *Pharmacol. Res.*, 2015, **102**, 123–131.
28 P. Wang, F. Yang, H. Yang, X. Xu, D. Liu, W. Xue and F. Zhu, *Bio-Med. Mater. Eng.*, 2015, **26**(suppl 1), S2233–2239.
29 T. Heinrich, H. Bottcher, R. Gericke, G. D. Bartoszyk, S. Anzali, C. A. Seyfried, H. E. Greiner and C. van Amsterdam, *J. Med. Chem.*, 2004, **47**, 4684–4692.
30 N. T. Hatzenbuhler, R. Baudy, D. A. Evrard, A. Failli, B. L. Harrison, S. Lenicek, R. E. Mewshaw, A. Saab, U. Shao, J. Sze, M. Zhang, D. Zhou, M. Chlenov, M. Kagan, J. Golembieski, G. Hornby, M. Lai and D. L. Smith, *J. Med. Chem.*, 2008, **51**, 6980–7004.
31 E. Dale, B. Bang-Andersen and C. Sanchez, *Biochem. Pharmacol.*, 2015, **95**, 81–97.
32 J. Martínez, S. Pérez, A. M. Oficialdegui, B. Heras, L. Orús, H. Villanueva, J. A. Palop, J. Roca, M. Mourelle, A. Bosch, J. C. Del Castillo, B. Lasheras, R. Tordera, J. del Río and A. Monge, *Eur. J. Med. Chem.*, 2001, **36**, 55–61.
33 A. Chodkowski, M. Z. Wrobel, J. Turlo, J. Kleps, A. Siwek, G. Nowak, M. Belka, T. Baczek, A. P. Mazurek and F. Herold, *Eur. J. Med. Chem.*, 2015, **90**, 21–32.
34 A. Gomolka, A. Ciesielska, M. Z. Wrobel, A. Chodkowski, J. Kleps, M. Dawidowski, A. Siwek, M. Wolak, K. Stachowicz, A. Slawinska, G. Nowak, G. Satala, A. J. Bojarski, M. Belka, S. Ulenberg, T. Baczek, P. Skowronek, J. Turlo and F. Herold, *Eur. J. Med. Chem.*, 2015, **98**, 221–236.
35 B. Li, J. Tang, Q. Yang, S. Li, X. Cui, Y. Li, Y. Chen, W. Xue, X. Li and F. Zhu, *Nucleic Acids Res.*, 2017, **45**, W154–W161.
36 B. Li, J. Tang, Q. Yang, X. Cui, S. Li, S. Chen, Q. Cao, W. Xue, N. Chen and F. Zhu, *Sci. Rep.*, 2016, **6**, 38881.
37 C. R. Hopkins, *ACS Chem. Neurosci.*, 2011, **2**, 554.
38 L. Tritschler, D. Felice, R. Colle, J. P. Guilloux, E. Corruble, A. M. Gardier and D. J. David, *Expert Rev. Clin. Pharmacol.*, 2014, **7**, 731–745.
39 O. M. Becker, D. S. Dhanoa, Y. Marantz, D. L. Chen, S. Shacham, S. Cheruku, A. Heifetz, P. Mohanty, M. Fichman,

A. Sharadendu, R. Nudelman, M. Kauffman and S. Noiman, *J. Med. Chem.*, 2006, **49**, 3116–3135.
40 C. Sanchez, K. E. Asin and F. Artigas, *Pharmacol. Ther.*, 2015, **145**, 43–57.
41 K. R. Connolly and M. E. Thase, *Expert Opin. Pharmacother.*, 2016, **17**, 421–431.
42 F. Zhu, C. Qin, L. Tao, X. Liu, Z. Shi, X. Ma, J. Jia, Y. Tan, C. Cui, J. Lin, C. Tan, Y. Jiang and Y. Chen, *Proc. Natl. Acad. Sci. U. S. A.*, 2011, **108**, 12943–12948.
43 F. Zhu, X. H. Ma, C. Qin, L. Tao, X. Liu, Z. Shi, C. L. Zhang, C. Y. Tan, Y. Z. Chen and Y. Y. Jiang, *PLoS One*, 2012, **7**, e39782.
44 H. Koldso, A. B. Christiansen, S. Sinning and B. Schiott, *ACS Chem. Neurosci.*, 2013, **4**, 295–309.
45 W. Xue, P. Wang, B. Li, Y. Li, X. Xu, F. Yang, X. Yao, Y. Z. Chen, F. Xu and F. Zhu, *Phys. Chem. Chem. Phys.*, 2016, **18**, 3260–3271.
46 J. A. Coleman, E. M. Green and E. Gouaux, *Nature*, 2016, **532**, 334–339.
47 J. Xu, P. Wang, H. Yang, J. Zhou, Y. Li, X. Li, W. Xue, C. Yu, Y. Tian and F. Zhu, *BioMed Res. Int.*, 2016, **2016**, 2509385.
48 F. Yang, T. Fu, X. Zhang, J. Hu, W. Xue, G. Zheng, B. Li, Y. Li, X. Yao and F. Zhu, *Mol. Simul.*, 2017, **43**, 1089–1098.
49 F. Zhu, L. Han, C. Zheng, B. Xie, M. T. Tammi, S. Yang, Y. Wei and Y. Chen, *J. Pharmacol. Exp. Ther.*, 2009, **330**, 304–315.
50 S. G. Rasmussen, B. T. DeVree, Y. Zou, A. C. Kruse, K. Y. Chung, T. S. Kobilka, F. S. Thian, P. S. Chae, E. Pardon, D. Calinski, J. M. Mathiesen, S. T. Shah, J. A. Lyons, M. Caffrey, S. H. Gellman, J. Steyaert, G. Skiniotis, W. I. Weis, R. K. Sunahara and B. K. Kobilka, *Nature*, 2011, **477**, 549–555.
51 K. Arnold, L. Bordoli, J. Kopp and T. Schwede, *Bioinformatics*, 2006, **22**, 195–201.
52 M. A. Larkin, G. Blackshields, N. P. Brown, R. Chenna, P. A. McGettigan, H. McWilliam, F. Valentin, I. M. Wallace, A. Wilm, R. Lopez, J. D. Thompson, T. J. Gibson and D. G. Higgins, *Bioinformatics*, 2007, **23**, 2947–2948.
53 X. Robert and P. Gouet, *Nucleic Acids Res.*, 2014, **42**, W320–W324.
54 R. A. Laskowski, *J. Appl. Crystallogr.*, 1993, **26**, 283–291.
55 *Glide, version 5.5*, Schrödinger, LLC, New York, 2009.
56 G. A. Kaminski, R. A. Friesner, J. Tirado-Rives and W. L. Jorgensen, *J. Phys. Chem. B*, 2001, **105**, 6474–6487.
57 M. P. Jacobson, D. L. Pincus, C. S. Rapp, T. J. Day, B. Honig, D. E. Shaw and R. A. Friesner, *Proteins*, 2004, **55**, 351–367.
58 M. A. Lomize, I. D. Pogozheva, H. Joo, H. I. Mosberg and A. L. Lomize, *Nucleic Acids Res.*, 2012, **40**, D370–D376.
59 E. L. Wu, X. Cheng, S. Jo, H. Rui, K. C. Song, E. M. Davila-Contreras, Y. Qi, J. Lee, V. Monje-Galvan, R. M. Venable, J. B. Klauda and W. Im, *J. Comput. Chem.*, 2014, **35**, 1997–2004.
60 D. A. Case, V. Babin, J. T. Berryman, R. M. Betz, Q. Cai, D. S. Cerutti, T. E. Cheatham, R. E. T. A. Darden, H. G. Duke, A. W. Goetz, S. Gusarov, N. Homeyer, P. Janowski, J. Kaus, I. Kolossváry, A. Kovalenko, T. S. Lee, S. LeGrand, T. Luchko, R. Luo, B. Madej, K. M. Merz, F. Paesani, D. R. Roe, A. Roitberg, C. Sagui, R. Salomon-Ferrer, G. Seabra, C. L. Simmerling, W. Smith, J. Swails, R. C. Walker, J. Wang, R. M. Wolf, X. Wu and P. A. Kollman, *AMBER 14*, University of California, San Francisco, 2014.
61 J. A. Maier, C. Martinez, K. Kasavajhala, L. Wickstrom, K. E. Hauser and C. Simmerling, *J. Chem. Theory Comput.*, 2015, **11**, 3696–3713.
62 C. J. Dickson, B. D. Madej, A. A. Skjevik, R. M. Betz, K. Teigen, I. R. Gould and R. C. Walker, *J. Chem. Theory Comput.*, 2014, **10**, 865–879.
63 W. L. Jorgensen, J. Chandrasekhar, J. D. Madura, R. W. Impey and M. L. Klein, *J. Chem. Phys.*, 1983, **79**, 926–935.
64 I. S. Joung, I. Thomas and E. Cheatham, *J. Phys. Chem. B*, 2008, **112**, 9020–9041.
65 J. Wang, W. Wang, P. A. Kollman and D. A. Case, *J. Mol. Graphics Modell.*, 2006, **25**, 247–260.
66 J. Wang, R. M. Wolf, J. W. Caldwell, P. A. Kollman and D. A. Case, *J. Comput. Chem.*, 2004, **25**, 1157–1174.
67 C. I. Bayly, P. Cieplak, W. D. Cornell and P. A. Kollman, *J. Phys. Chem.*, 1993, **97**, 10269–10280.
68 T. Darden, D. York and L. Pedersen, *J. Chem. Phys.*, 1993, **98**, 10089–10092.
69 L. Larini, R. Mannella and D. Leporini, *J. Chem. Phys.*, 2007, **126**, 104101.
70 A. Onufriev, D. Bashford and D. A. Case, *Proteins*, 2004, **55**, 383–394.
71 J. Weiser, P. S. Shenkin and W. C. Still, *J. Comput. Chem.*, 1999, **20**, 217–230.
72 S. Tippmann, *Nature*, 2015, **517**, 109–110.
73 G. J. Szekely and M. L. Rizzo, *J. Classif.*, 2005, **22**, 151–183.
74 I. Letunic and P. Bork, *Nucleic Acids Res.*, 2016, **44**, W242–W245.
75 I. S. Moreira, P. A. Fernandes and M. J. Ramos, *J. Comput. Chem.*, 2007, **28**, 644–654.
76 I. Massova and P. A. Kollman, *J. Am. Chem. Soc.*, 1999, **121**, 8133–8143.
77 X. Q. Yang, J. Y. Liu, X. C. Li, M. H. Chen and Y. L. Zhang, *J. Chem. Inf. Model.*, 2014, **54**, 1356–1370.
78 V. Katritch, M. Rueda, P. C. H. Lam, M. Yeager and R. Abagyan, *Proteins*, 2010, **78**, 197–211.
79 P. Lian, L. Li, C. Geng, X. Zhen and W. Fu, *J. Chem. Inf. Model.*, 2015, **55**, 1616–1627.
80 C. Wang, Y. Jiang, J. M. Ma, H. X. Wu, D. Wacker, V. Katritch, G. W. Han, W. Liu, X. P. Huang, E. Vardy, J. D. McCorvy, X. Gao, X. E. Zhou, K. Melcher, C. H. Zhang, F. Bai, H. Y. Yang, L. L. Yang, H. L. Jiang, B. L. Roth, V. Cherezov, R. C. Stevens and H. E. Xu, *Science*, 2013, **340**, 610–614.
81 L. Xu, Y. Zhang, L. Zheng, C. Qiao, Y. Li, D. Li, X. Zhen and T. Hou, *J. Med. Chem.*, 2014, **57**, 3737–3745.
82 J. Shonberg, R. C. Kling, P. Gmeiner and S. Lober, *Bioorg. Med. Chem.*, 2015, **23**, 3880–3906.
83 J. Du, H. Sun, L. Xi, J. Li, Y. Yang, H. Liu and X. Yao, *J. Comput. Chem.*, 2011, **32**, 2800–2809.
84 M. Shen, S. Zhou, Y. Li, P. Pan, L. Zhang and T. Hou, *Mol. BioSyst.*, 2013, **9**, 361–374.

85 H. B. Rao, F. Zhu, G. B. Yang, Z. R. Li and Y. Z. Chen, *Nucleic Acids Res.*, 2011, **39**, W385–W390.
86 H. Sun, P. Chen, D. Li, Y. Li and T. Hou, *J. Chem. Theory Comput.*, 2016, **12**, 851–860.
87 Z. Wang, H. Sun, X. Yao, D. Li, L. Xu, Y. Li, S. Tian and T. Hou, *Phys. Chem. Chem. Phys.*, 2016, **18**, 12964–12975.
88 D. M. Rosenbaum, C. Zhang, J. A. Lyons, R. Holl, D. Aragao, D. H. Arlow, S. G. Rasmussen, H. J. Choi, B. T. Devree, R. K. Sunahara, P. S. Chae, S. H. Gellman, R. O. Dror, D. E. Shaw, W. I. Weis, M. Caffrey, P. Gmeiner and B. K. Kobilka, *Nature*, 2011, **469**, 236–240.
89 G. Zheng, W. Xue, P. Wang, F. Yang, B. Li, X. Li, Y. Li, X. Yao and F. Zhu, *Sci. Rep.*, 2016, **6**, 26883.
90 H. Sun, S. Tian, S. Zhou, Y. Li, D. Li, L. Xu, M. Shen, P. Pan and T. Hou, *Sci. Rep.*, 2015, **5**, 8457.
91 T. Hou, J. Wang, Y. Li and W. Wang, *J. Chem. Inf. Model.*, 2011, **51**, 69–82.
92 L. Xu, H. Sun, Y. Li, J. Wang and T. Hou, *J. Phys. Chem. B*, 2013, **117**, 8408–8421.
93 H. Sun, Y. Li, M. Shen, S. Tian, L. Xu, P. Pan, Y. Guan and T. Hou, *Phys. Chem. Chem. Phys.*, 2014, **16**, 22035–22045.
94 F. Chen, H. Liu, H. Sun, P. Pan, Y. Li, D. Li and T. Hou, *Phys. Chem. Chem. Phys.*, 2016, **18**, 22129–22139.
95 B. Y. Ho, A. Karschin, T. Branchek, N. Davidson and H. A. Lester, *FEBS Lett.*, 1992, **312**, 256–262.
96 A. Tarcsay and G. M. Keseru, *Drug Discovery Today*, 2015, **20**, 86–94.
97 F. Zhu, L. Y. Han, X. Chen, H. H. Lin, S. Ong, B. Xie, H. L. Zhang and Y. Z. Chen, *Curr. Protein Pept. Sci.*, 2008, **9**, 70–95.
98 H. Sun, Y. Li, S. Tian, J. Wang and T. Hou, *PLoS Comput. Biol.*, 2014, **10**, e1003729.
99 C. Bissantz, B. Kuhn and M. Stahl, *J. Med. Chem.*, 2010, **53**, 5061–5084.
100 S. Dilly and J. F. Liegeois, *J. Chem. Inf. Model.*, 2016, **56**, 1324–1331.
101 J. F. Liegeois, M. Lespagnard, E. Meneses Salas, F. Mangin, J. Scuvee-Moreau and S. Dilly, *ACS Med. Chem. Lett.*, 2014, **5**, 358–362.
102 S. Yuan, Q. Peng, K. Palczewski, H. Vogel and S. Filipek, *Angew. Chem., Int. Ed.*, 2016, **55**, 8661–8665.
103 F. Zhu, C. J. Zheng, L. Y. Han, B. Xie, J. Jia, X. Liu, M. T. Tammi, S. Y. Yang, Y. Q. Wei and Y. Z. Chen, *Curr. Mol. Pharmacol.*, 2008, **1**, 213–232.
104 H. C. Chan, S. Filipek and S. Yuan, *Sci. Rep.*, 2016, **6**, 34736.
105 C. Munk, K. Harpsoe, A. S. Hauser, V. Isberg and D. E. Gloriam, *Curr. Opin. Pharmacol.*, 2016, **30**, 51–58.

